

# Separating double-beta decay events from solar neutrino interactions in kiloton-scale liquid scintillator detectors

Andrey Elagin<sup>1</sup>, Henry Frisch<sup>1</sup>, Lindley Winslow<sup>2</sup>, *et al* (**opt-in**)

<sup>1</sup>*Enrico Fermi Institute, University of Chicago*

<sup>2</sup>*Massachusetts Institute of Technology*

## Abstract

We propose a technique for separating  $0\nu\beta\beta$ -decay events from background due to  ${}^8B$  solar neutrino interactions in a liquid scintillator detector. The technique compares event topology of the signal and background events using spherical harmonics analysis of the early light emitted in  $0\nu\beta\beta$ -decay and  ${}^8B$  events. Selection of early photons using fast photo-detectors allows for separation of directional Cherenkov from isotropic scintillation light and identification of two event topologies based on the spatial distribution of the early photons in the detector.

19	<b>Contents</b>	
20	<b>1 Introduction</b>	<b>3</b>
21	<b>2 Detector Model</b>	<b>5</b>
22	<b>3 Spherical Harmonics Analysis</b>	<b>6</b>
23	3.1 Event Topology and Spherical Harmonics . . . . .	6
24	3.2 Mathematical description of spherical harmonics analysis . . . . .	8
25	3.3 Software and implementation of the spherical harmonics analysis . . . .	12
26	<b>4 Performance and Experimental Challenges</b>	<b>15</b>
27	4.1 Performance of the spherical harmonics analysis on $0\nu\beta\beta$ -decay and ${}^8B$	
28	events. . . . .	15
29	4.2 Experimental challenges . . . . .	16
30	<b>5 Conclusions</b>	<b>22</b>
31	<b>6 Acknowledgments</b>	<b>22</b>
32	<b>A <math>0\nu\beta\beta</math>-decay vs <math>{}^{10}C</math> background</b>	<b>22</b>

# 1 Introduction

Introductory paragraphs saying that  $0\nu\beta\beta$ -decay is important and we'd like to improve sensitivity of liquid scintillator detectors.

In a large liquid scintillator detector two dominant backgrounds to  $0\nu\beta\beta$ -decay signal are  $2\nu\beta\beta$ -decay and CCQE interactions of  ${}^8\text{B}$  solar neutrinos. As an example we show simulation of the energy spectrum for the  $0\nu\beta\beta$ -decay signal and various backgrounds in SNO+ experiment in Fig. 1.

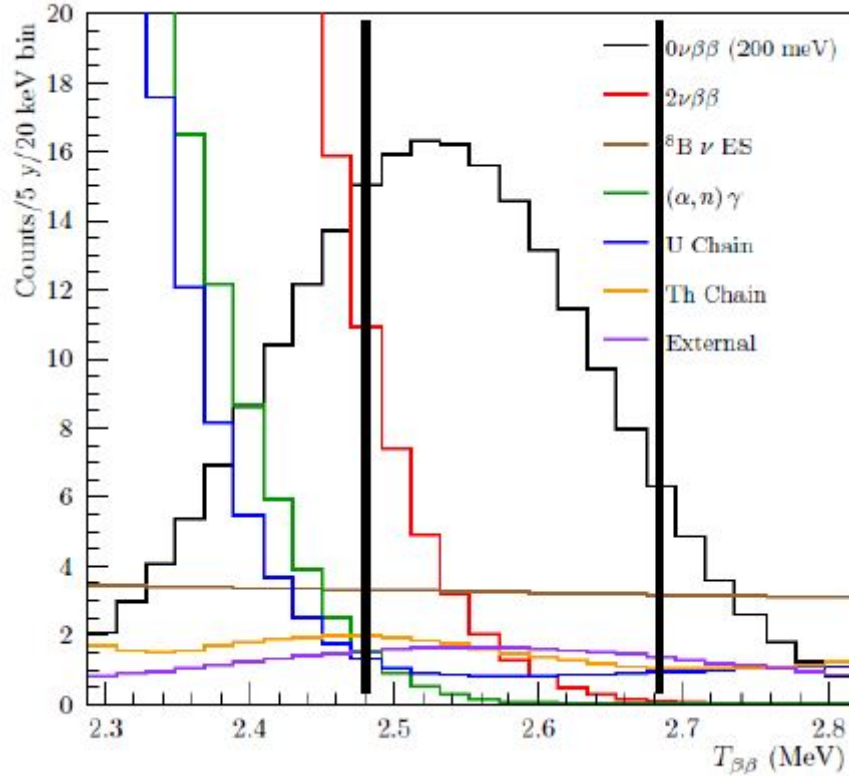


Figure 1: SNO+ Phase I signal and background energy spectrum (visible kinetic energy reconstructed under a  $0\nu\beta\beta$  hypothesis). Plot taken from [2]

As shown in Fig. 2, in the region of interest (ROI) where total kinetic energy of the electrons is close to the energy spectrum end point (Q-value), there is almost no difference in kinematic distributions between  $0\nu\beta\beta$ - and  $2\nu\beta\beta$ -decays. The event topology of these two processes are very similar - both produce two electron tracks in

the detector. Therefore the energy resolution is the key parameter for discrimination between  $0\nu\beta\beta$ - and  $2\nu\beta\beta$ -decays in any detector searching for  $0\nu\beta\beta$ -decay.

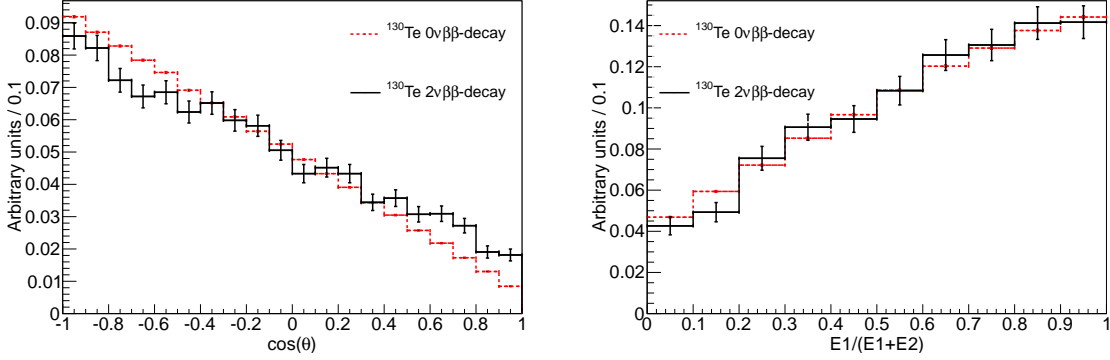


Figure 2: Comparison between kinematics of  $0\nu\beta\beta$ - (dashed red lines) and  $2\nu\beta\beta$ -decays (solid black lines) for events with the total kinetic energy of the electrons above 90% of the Q-value. (Left) Cosine of the angle between two electrons. (Right) Fraction of energy carried by one of the two electrons. Due to limited statistic around the energy spectrum end point for  $2\nu\beta\beta$ -decay we show statistical errors for each bin.

While the event topology of  $2\nu\beta\beta$ -decay is very similar to the  $0\nu\beta\beta$ -decay, the topology of the next largest background coming from the  $^8\text{B}$  solar neutrino is sufficiently different and can be used to suppress this type of background.

$^8\text{B}$  solar neutrino interactions produce only one electron. In a liquid scintillator detector the difference between two electrons and one electron will show up in the distribution of the Cherenkov photons. Abundant scintillation light makes it challenging to extract small Cherenkov light contribution from low energy electrons. However, as have been shown in our previous work, photo-detectors with time resolution of  $\sim 100$  ps can allow for selection of photons that contain significant fraction of Cherenkov light produced by 1-5 MeV electrons in a kilo-ton scale liquid scintillator detector. Cherenkov photons on average arrive to the detector surface earlier than scintillation light due to longer wavelength of the Cherenkov photons and a delay in the scintillation process. Thus early light primarily consist of Cherenkov photons.

In this paper we propose to use spherical harmonics to analyze distributions of the early photo-electrons (PE) for discrimination between  $^8\text{B}$  background and  $0\nu\beta\beta$ -decay

61 signal.

62 Section 2 describes our detector model. Section 3 introduces spherical harmonics  
 63 analysis. Performance and experimental challenges are discussed in Sec. 4

## 64 2 Detector Model

65 Copy info from [1].

66 Figures 3 and 4 show simulation output relevant for further discussion.

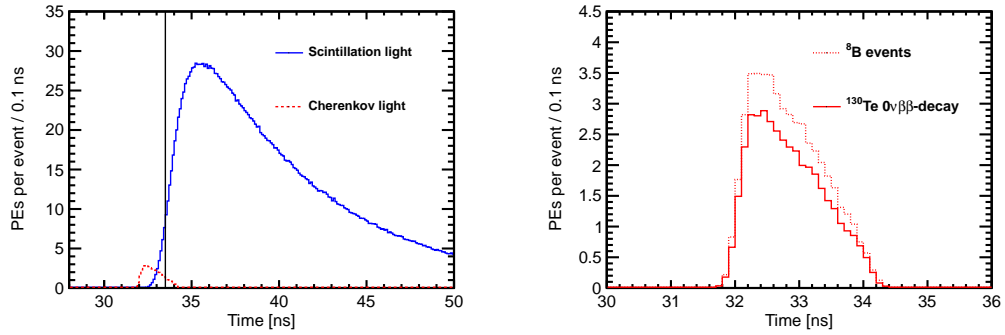


Figure 3: (Left) Photo-electron (PE) arrival times after application of the photo-detector transit time spread (TTS) of 100 ps for the simulation of 1000  $0\nu\beta\beta$ -decay events of  $^{130}\text{Te}$  at the center of the detector. PEs from Cherenkov light (red, dash line) and scintillation light (blue, solid line) are compared. The black vertical line illustrates a time cut at 33.5 ns. (Right) Comparison between Cherenkov PEs arrival time for  $^{130}\text{Te}$   $0\nu\beta\beta$ -decay (solid line) and  $^8\text{B}$  (dotted line) events. **Distributions of the scintillation PEs arrival time are indistinguishable between  $^{130}\text{Te}$   $0\nu\beta\beta$ -decay and  $^8\text{B}$  due to identical total energy in the event,  $Q(^{130}\text{Te})=2.529$  MeV.**

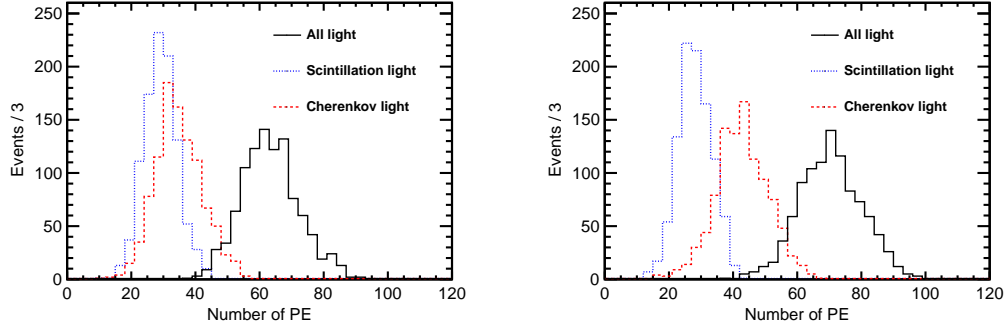


Figure 4: Number of Cherenkov (red dash line), scintillation (blue dotted line), and total (black solid line) PEs for the simulation of 1000  $^{130}\text{Te}$   $0\nu\beta\beta$ -decay (left panel) and  $^8\text{B}$  (right panel) events.

### 3 Spherical Harmonics Analysis

#### 3.1 Event Topology and Spherical Harmonics

Signature of the  $0\nu\beta\beta$ -decay is two electrons with total kinetic energy equal to the isotope Q-value (e.g., 2.529 MeV for  $^{130}\text{Te}$ ). These two electrons are often above Cherenkov threshold and therefore will produce two (fuzzy) rings of Cherenkov light on top of isotropic scintillation light.  $^8\text{B}$  background events have only one electron producing one Cherenkov ring.

In the detector regions where Cherenkov and scintillation light overlap the Cherenkov light on average arrives earlier due to a time delay in emission and a shorter wavelengths of the scintillation light. Therefore, while a vast majority of light produced in  $0\nu\beta\beta$ -decay events consists of scintillation photons, timing information can be used to select a sample of photons with high fraction of Cherenkov light.

Due to directional nature of the Cherenkov light the spatial distribution of early photons on the detector sphere will be different for the  $0\nu\beta\beta$ -decay signal and the background from  $^8\text{B}$  events.

The simplest case for spherical harmonics analysis are events with the vertex located exactly in the center of the detector. For such event Cherenkov and scintillation light can be separated by applying a time cut on the photon arrival time as demonstrated

85 in [1]. To introduce the technique of spherical harmonics analysis we will follow the  
 86 same strategy as in [1] and use central events with a slightly different cut on the photon  
 87 arrival time of 33.5 ns.

88 In order to illustrate the difference between different event topologies we introduce  
 89 three event topologies: two electrons produced back-to-back at  $180^\circ$  angle, two electrons  
 90 at  $90^\circ$  angle, and a single electron. The two former are representative topologies of  
 91 the  $0\nu\beta\beta$ -decay signal events and the latter represents  $^8B$  background events. Figure 5  
 92 shows Cherenkov photon distributions of 5 MeV electrons for each of the three topology.  
 93 100 events are overlayed in order to make Cherenkov rings visible.

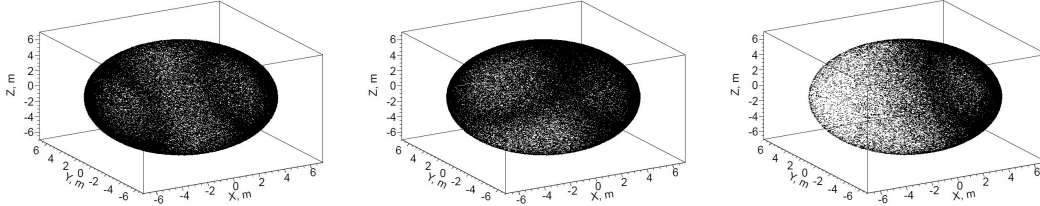


Figure 5: Cherenkov photons distributions on the detector sphere for the three representative event topologies: two back-to-back electrons (Left), two electrons at  $90^\circ$  angle (Middle), and a single electron (Center). All electrons are 5 MeV and originate at the center of the detector. 100 events overlayed for better visibility of the Cherenkov rings. 100% QE is assumed.

94 In practice Cherenkov rings from low energy electrons are not clearly visible. Fig-  
 95 ure 6 shows photons distribution for individual events from three topologies with total  
 96 kinetic energy of 2.529 MeV (Q-value of  $\text{Te130}$ ). Event topology can be identified by  
 97 looking at clusters of Cherenkov photons in different segments of the sphere.

98 Examples of three  $^{130}\text{Te}$   $0\nu\beta\beta$ -decay events simulated at the center of the detector  
 99 are shown in Fig. 7. Early PEs from Cherenkov and scintillation light are shown.  
 100 Default QE is used in the simulation. Time cut of 33.5 ns on the photon arrival time  
 101 is used to select early light. Uniformly distributed scintillation light make it more  
 102 difficult to guess the event topology. Nevertheless we show that there is still sufficient  
 103 difference in the position distribution of the early light to separate two track and single  
 104 track events.

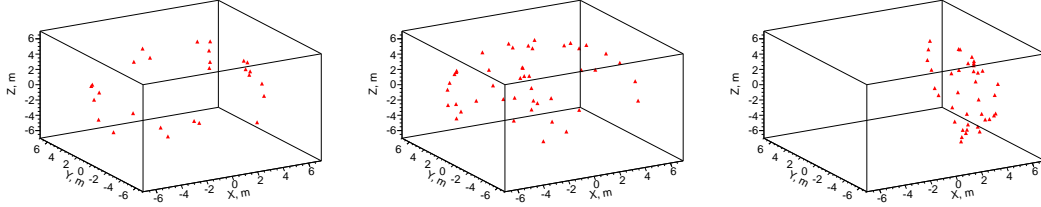


Figure 6: Cherenkov photons distributions on the detector sphere for the three representative event topologies: two back-to-back 1.26 MeV electrons (Left), two 1.26 MeV electrons at  $90^\circ$  angle (Middle), and a single 2.529 MeV electron (Center). All electrons originate at the center of the detector. One randomly selected event is chosen for each category. Default QE is applied.

105  $0\nu\beta\beta$ -decay events become indistinguishable from single track topology when the  
 106 angle between two electrons is small For quantitative description of the difference in  
 107 the event topology we analyze spherical harmonics of the photon distributions on the  
 108 detector sphere. We construct rotation invariant variables and compare them between  
 109 signal and background events. As it is shown in Fig. 7  $0\nu\beta\beta$ -decay become indistin-  
 110 guishable from single track topology when the angle between two electrons is small  
 111 (two degenerate tracks). Therefore the method of spherical harmonics is most effective  
 112 for events with large angular separation between the two tracks.

113 In this paper we focus on topological difference between two tracks and single track  
 114 events and do not make any attempt to use absolute directional information to suppress  
 115 single track events which direction is consistent with the direction from solar neutrinos.  
 116 Once a single track topology is established one can use a centroid method (see Ref. [1])  
 117 to reconstruct directionality of the track or two degenerate tracks and get rid of events  
 118 aligned with the direction of  $^8B$  solar neutrinos.

### 119 3.2 Mathematical description of spherical harmonics analysis

120 A function  $f(\theta, \phi)$  can be decomposed to a sum of spherical harmonics:



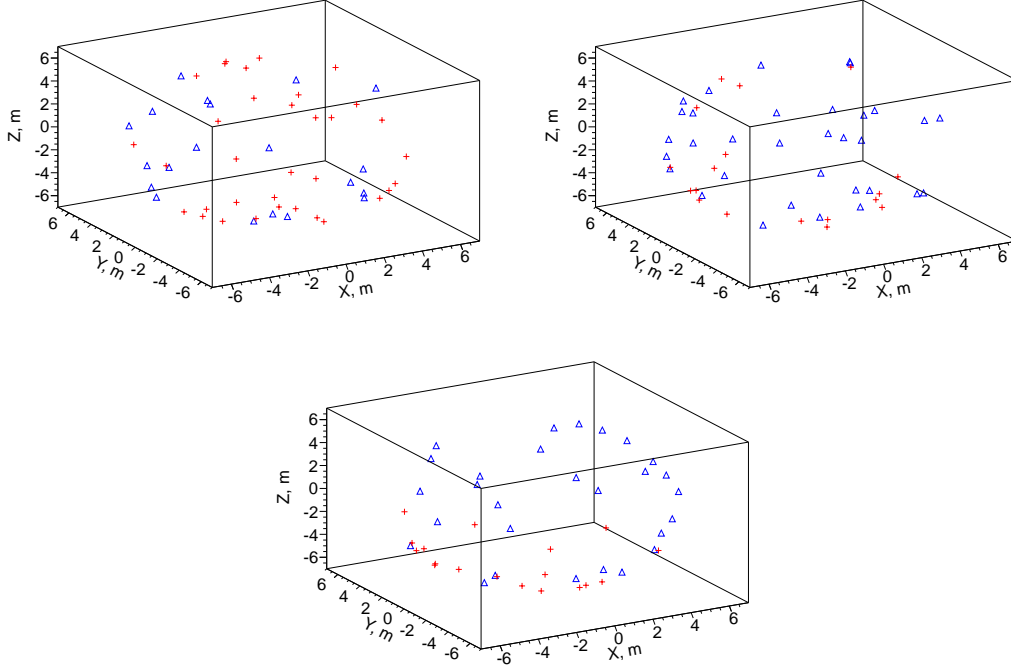


Figure 7: Examples of PEs position on the detector sphere after time cut of 33.5ns. PEs from Cherenkov (red) and scintillation light (blue) are compared. (Top left)  $^{130}\text{Te}$   $0\nu\beta\beta$ -decay back-to-back electrons:  $E_1=1.257$  MeV,  $E_2=1.270$  MeV,  $\cos(\theta)=-0.908$ . (Top right)  $^{130}\text{Te}$   $0\nu\beta\beta$ -decay electrons at  $\sim 90^\circ$ :  $E_1=1.264$  MeV,  $E_2=1.263$  MeV,  $\cos(\theta)=-0.029$ . (Bottom left)  $^{130}\text{Te}$   $0\nu\beta\beta$ -decay electrons at  $\sim 0^\circ$ :  $E_1=1.186$  MeV,  $E_2=1.340$  MeV,  $\cos(\theta)=0.888$ . (Bottom right) 2.529 MeV single electron. Events are simulated at the center of the detector. Default QE is applied.

$$f(\theta, \phi) = \sum_{l=0}^{\infty} \sum_{m=-l}^l f_{lm} Y_{lm}(\theta, \phi), \quad (1)$$

121 where  $Y_{lm}$  are Laplace's spherical harmonics defined in Eq. 2 in real-value basis  
122 using Legendre polynomials  $P_l$ . Coefficients  $f_{lm}$  are defined in Eq. 3

$$Y_{lm} = \text{LONGformulaHERE} \quad (2)$$

$$f_{lm} = \text{LONG formula HERE} \quad (3)$$

Equation 4 defines multiple moments  $S_l$  which are invariant under rotation. Combination of  $S_l$ 's for ( $l=0,1,2,\dots$ ) is determined by the event topology and can be used to distinguish between different topologies.

$$S_l = \sum_{m=-l}^{m=l} |f_{lm}|^2 \quad (4)$$

Figure 8 compares  $S_l$  distributions for two electrons emitted at 180 degree, two electrons at 90 degree, and a single electron. Total kinetic energy of the electrons is the same in all three cases.

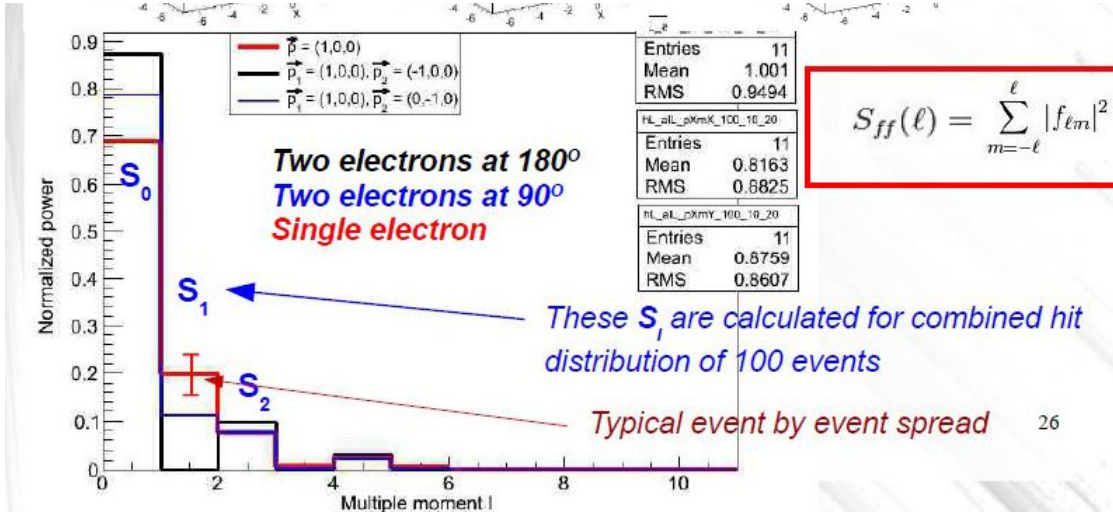


Figure 8: Average  $S_l$  values for two electrons at 180 degree (color1) and 90 degree (color2) 1.5 MeV each and a single electron (color3) with the energy of 3 MeV. Error bars are RMS values of each corresponding individual  $S_l$  distribution (each consists of 1000 events simulated at the center of the detector) indicating typical event-by-event variation.

In order to compare spherical harmonics for events with vertices located off-center anywhere inside the detector volume a coordinate transformation for each photon hit

131 is needed. The transformation applied for each photon hit within an event is shown  
 132 in Fig. 9. Solid circle schematically shows actual detector boundaries. Dotted circle  
 133 shows a new sphere of radius  $R=6.5$  m with the event vertex position in the center.  
 134 The radius vector of each photon hit is stretched or shorten until intersection with this  
 135 new sphere using transformation  $\vec{r}_{hit} = \frac{\vec{a}}{|\vec{a}|} \cdot R$ . Where  $\vec{r}_{hit}$  is a new radius vector of  
 136 the photon hit,  $R$  is detector sphere radius, and  $\vec{a} = \vec{r}_{hit} - \vec{r}_{vtx}$  with  $\vec{r}_{hit}$  and  $\vec{r}_{vtx}$  being  
 137 radius vectors of the photon hit and vertex position in original coordinates.

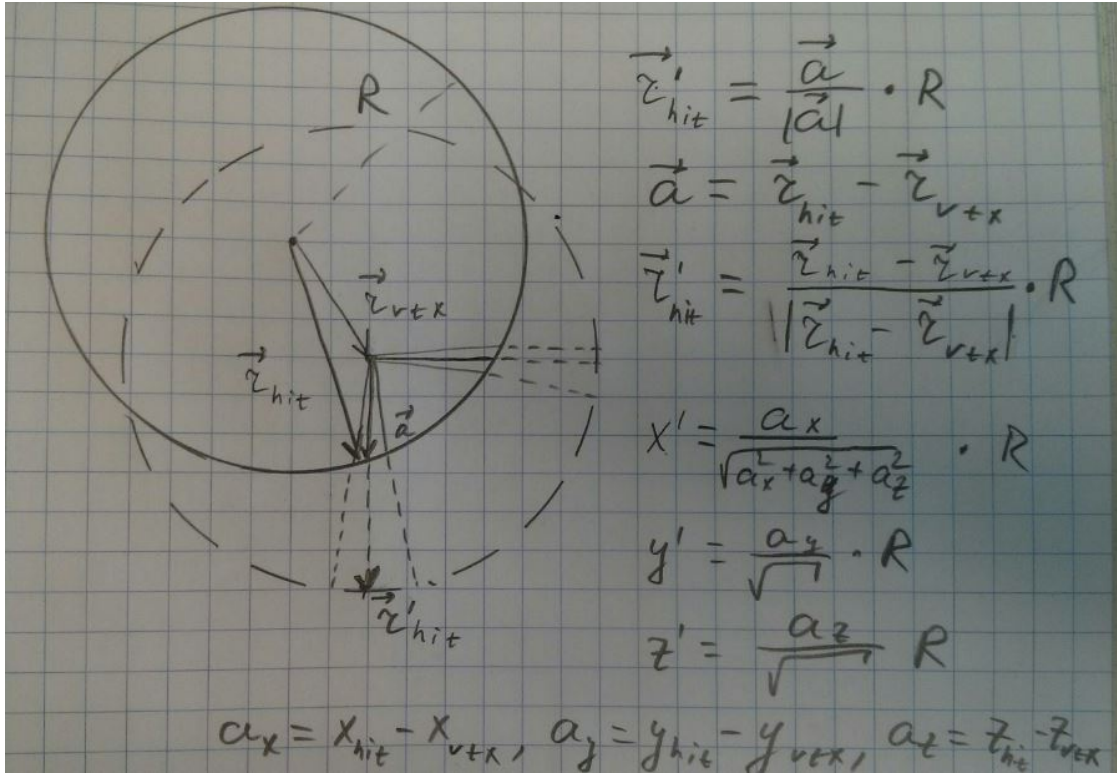


Figure 9: Coordinate transformation applied to events that are off-center. Solid circle schematically shows actual detector boundaries. Dotted circle shows a new sphere of radius  $R=6.5$  m with the event vertex position in the center. The radius vector of each photon hit is stretched or shorten until intersection with this new sphere using transformation  $\vec{r}_{hit} = \frac{\vec{a}}{|\vec{a}|} \cdot R$ . Where  $\vec{r}_{hit}$  is a new radius vector of the photon hit,  $R$  is detector sphere radius, and  $\vec{a} = \vec{r}_{hit} - \vec{r}_{vtx}$  with  $\vec{r}_{hit}$  and  $\vec{r}_{vtx}$  being radius vectors of the photon hit and vertex position in original coordinates and correspondingly.

### 3.3 Software and implementation of the spherical harmonics analysis

**A few words on the implementation. Calculation of  $S_l$ 's requires numerical integration that needs to be explained.**

To illustrate spherical harmonics analysis technique we compare distributions of  $S_0$ ,  $S_1$ ,  $S_2$ , and  $S_3$  for the three representative event topologies described in Sec. 3.1. Almost all the information about event topology is carried by Cherenkov light. Therefore we first show spherical harmonics of back-to-back,  $90^\circ$  and single track topologies calculated using Cherenkov light only (see Fig. 10). No QE is applied here.

Two top panels of Fig. 10 show 2-dimensional distributions,  $S_0$  vs  $S_1$  and  $S_2$  vs  $S_3$ , to demonstrate that all four  $S_l$ 's provide separation between event topologies. We also introduce a 1-dimensional variable,  $S_{01}$  (bottom panel of Fig. 10), that has the best separation power for majority of event topologies considered in this paper.  $S_{01}$  is defined as a projection of  $S_1$  vs  $S_2$  distribution onto a linear fit of this 2-D distribution.

The effects from scintillation light and applying default QE is shown in Fig. 11. Spherical harmonics of the same three representative event topologies are now calculated using early light (photons with arrival time less than 33.5 ns) that contains both directional Cherenkov light and uniform scintillation light. Default QE is also applied. Higher order multiple moments,  $S_2$  and  $S_3$ , no longer provide noticeable separation between different event topologies.

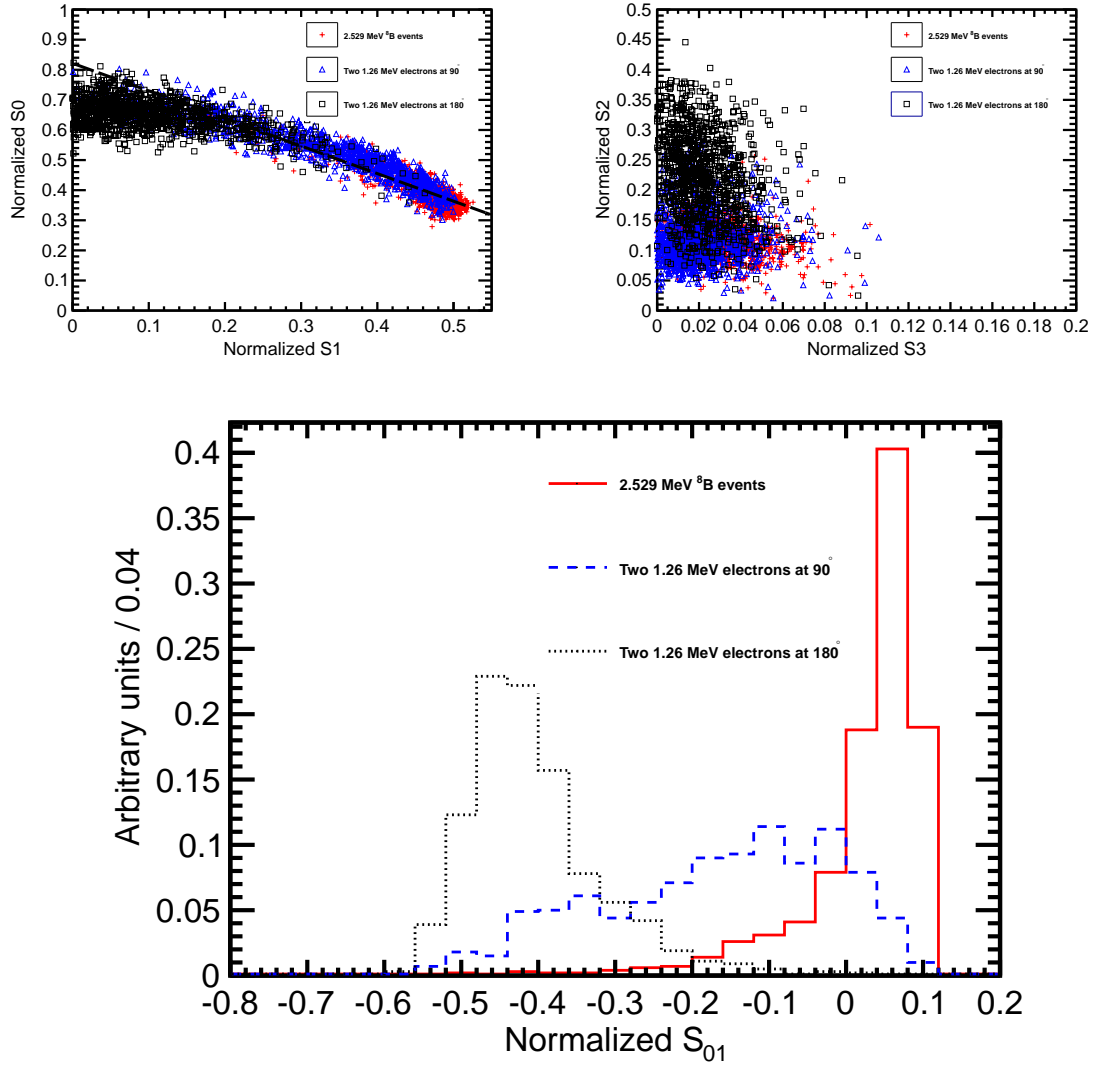


Figure 10: Spherical harmonics for three event topologies: two back-to-back 1.26 MeV electrons (black squares and black dotted line), two 1.26 MeV electrons at  $90^\circ$  angle (blue triangles and blue dashed line), and a single 2.529 MeV electron representing  ${}^8\text{B}$  background (red crosses and red solid line). Simulation of 1000 events originated at the center of the sphere. Perfect separation between Cherenkov and scintillation light is implemented in this simulation by using only Cherenkov photons. (Top left)  $S_0$  versus  $S_1$  scatter plot. Black dotted line is a linear fit of the  $90^\circ$  topology and  ${}^8\text{B}$  events. Variable  $S_{01}$  is defined as a projection of 2D distribution onto this linear fit. (Top right)  $S_2$  versus  $S_3$  scatter plot. (Bottom)  $S_{01}$  distributions for the three topologies. These distributions are normalized to unit area for shape comparison

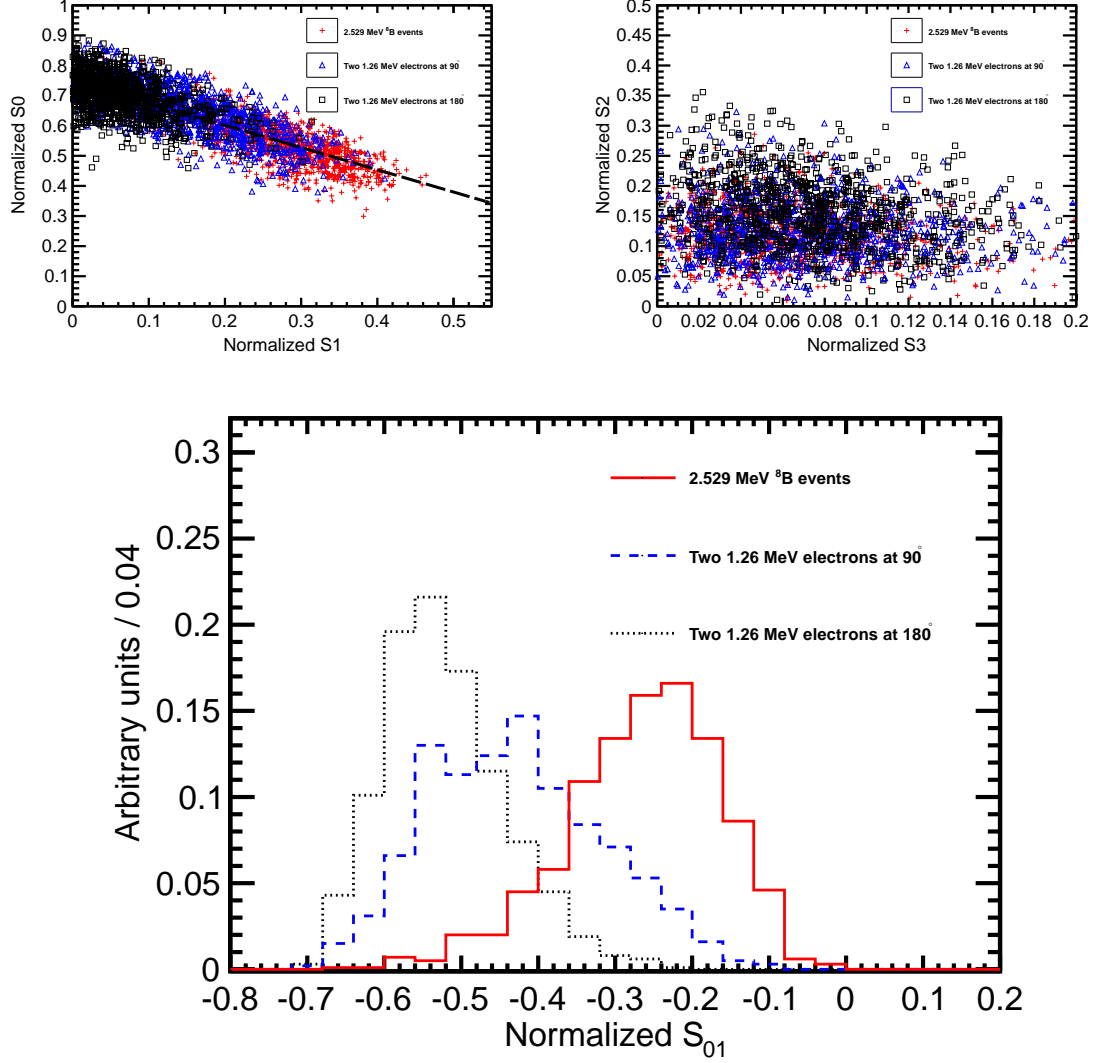


Figure 11: Spherical harmonics for three event topologies: two back-to-back 1.26 MeV electrons (black squares and black dotted line), two 1.26 MeV electrons at  $90^\circ$  angle (blue triangles and blue dashed line), and a single 2.529 MeV electron representing  ${}^8\text{B}$  background (red crosses and red solid line). Simulation of 1000 events originated at the center of the sphere. Separation between Cherenkov and scintillation light is implemented 33.5 ns cut on the photon arrival time. Perfect vertex reconstruction - true vertex position is used. (Top left)  $S_0$  versus  $S_1$  scatter plot. Black dotted line is a linear fit of the  $90^\circ$  topology and  ${}^8\text{B}$  events. Variable  $S_{01}$  is defined as a projection of 2D distribution onto this linear fit. (Top right)  $S_2$  versus  $S_3$  scatter plot. (Bottom)  $S_{01}$  distributions for the three topologies. These distributions are normalized to unit area for shape comparison

## 4 Performance and Experimental Challenges

### 4.1 Performance of the spherical harmonics analysis on $0\nu\beta\beta$ -decay and ${}^8B$ events.

Comparison of  $S_0$  and  $S_1$  distributions between  $0\nu\beta\beta$ -decay and  ${}^8B$  events is shown in Fig. 12. There is a noticeable separation between the signal and background. We also note that in the energy range of interest  $S_l$ 's do not have strong dependence on the energy deposited in the detector, which makes them reliable discriminators at the endpoint of the  $0\nu\beta\beta$ -decay energy spectrum. The information about the event topology is complimentary to the energy measurements.

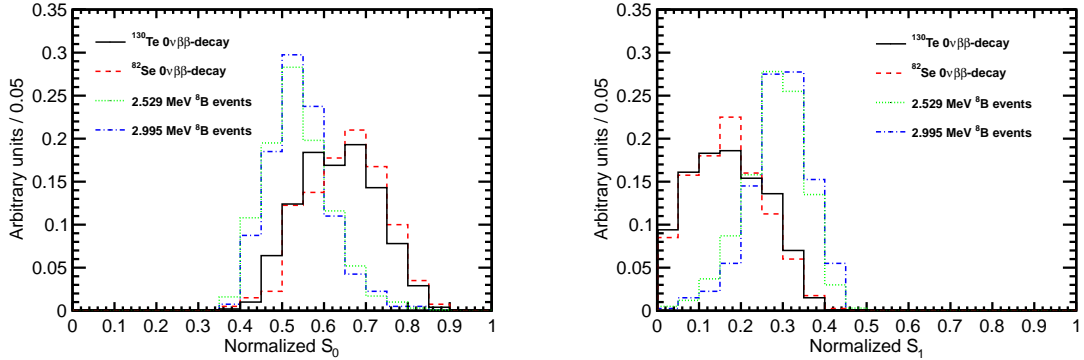


Figure 12:  $S_0$  (left) and  $S_1$  (right) distributions for events with two different event topologies and total kinetic energy.  ${}^{130}\text{Te}$ ,  ${}^{82}\text{Se}$   $0\nu\beta\beta$ -decay, 2.529 MeV and 2.995 MeV events are compared. The simulation is done for events with the vertex in the center of the detector.  ${}^8B$  events are implemented as 2.529 MeV or 2.995 MeV electrons with initial direction along  $x$ -axis. Perfect vertex reconstruction - true vertex position is used. Time cut of 33.5 ns on the photon arrival time is applied.

Figure 13 shows separation between  ${}^{130}\text{Te}$  signal and  ${}^8B$  background events simulated at the center of the detector. True values of vertex position and time is used. Time cut of 33.5 ns on the photon arrival time is applied to separate Cherenkov and scintillation light. Most of the discrimination between signal and background comes from  $S_0$  and  $S_1$ . In the following  $S_2$  and  $S_3$  are not used to separate  ${}^{130}\text{Te}$  and  ${}^8B$

172 events<sup>1</sup>. The scatter plot of  $S_2$  vs  $S_3$  is shown here for completeness.

173 In order to optimize separation between  $^{130}\text{Te}$  signal and  $^8\text{B}$  background a linear  
174 combination of  $S_0$  and  $S_1$ ,  $S_{01}$ , is used. A linear fit,  $S_0 = A \times S_1 + B$ , of 2-dimensional  $S_0$   
175 vs  $S_1$  scatter plot is performed as shown in Fig. 13. Then this 2-dimensional distribution  
176 is projected onto the fitted line. **A little bit of math here to quantitatively**  
177 **describe  $S_{01}$  via  $S_0$  and  $S_1$ :** A new coordinate frame is obtained by rotation of the  
178 original  $S_0$ - $S_1$  frame at angle  $\theta$  obtained from the fit:  $\tan(\theta)=A$ . A transformation,  
179  $S_{01} = S_1 \cdot \cos(\theta) + S_0 \cdot \sin(\theta)$ , defines the  $S_{01}$  variable.

180 Bottom plot in Fig. 13 shows performance of the  $S_{01}$  variable to separate  $^{130}\text{Te}$   
181 signal and  $^8\text{B}$  background. A fit to this distribution can be done to optimize the  
182 discrimination power in a particular experimental settings. Here we refrain from quan-  
183 titative estimates on the improvements in sensitivity to  $0\nu\beta\beta$ -decay search using this  
184 method of spherical harmonics as a reliable estimate would require a dedicated analysis  
185 taking into account all the details of a particular experiment.

## 186 4.2 Experimental challenges

187 So far only events at the center of the detector have been considered. In this sec-  
188 tion we discuss performance of the spherical harmonics analysis for events distributed  
189 within the fiducial volume of the detector taking into account finite resolution on vertex  
190 position reconstruction.

191 When the vertex is not at the center, a uniform time cut on the photon arrival  
192 time is no longer effective in the selection of Cherenkov photons. In the case of off-  
193 center vertex, even significantly delayed scintillation photons can reach the side of the  
194 detector that is closer to the vertex much earlier than Cherenkov photons traveling to  
195 the opposite side of the detector. Therefore, the time cut has to be position dependent  
196 and take into account the total distance traveled by each individual photon.

197 We found that the time cut defined as  $\Delta t = t_{measured}^{phot} - t_{predicted}^{phot} < 1$  ns selects pho-

---

<sup>1</sup> $S_2$  and  $S_3$  are helpful for separation of  $^{130}\text{Te}$  signal from  $^{10}\text{C}$  background. See Appendix.



tons with sufficient fraction of Cherenkov photons. Predicted time,  $t_{predicted}^{phot}=l/v^{phot}$ , depends on total distance,  $l$ , traveled by the photon and proper assignment of the velocity for each photon,  $v^{phot}$ , that depends on index of refraction<sup>2</sup>. Therefore the relative Cherenkov/scintillation composition of the light selected with this  $\Delta t$  time cut depends on the vertex location and chromatic dispersions.

Due to chromatic dispersion, even with perfect vertex reconstruction one cannot achieve the same level of separation between Cherenkov and scintillation light compared to the central events considered above in Section 4. This in turn reduces the effectiveness of the spherical harmonics analysis in separating of  $0\nu\beta\beta$ -decay and  ${}^8B$  events (see Fig. 14). However next generation detectors can recover losses due to chromatic dispersion by choosing liquid scintillators with a more narrow emission spectrum.

Imprecise knowledge of the vertex position due to finite resolution is another factor affecting performance of the spherical harmonics analysis. Small deviations in vertex reconstruction cause large effect on  $S_0$  and  $S_1$  for single electron event topology. For the vertices shifted along the direction of the electron the  $\Delta t$  cut makes uniform scintillation light distribution less uniform. The  $\Delta t$  cut selects more forward emitted photons in the case when the reconstructed vertex is shifted to the direction opposite to the electron momentum (enhancing forward region populated by Cherenkov photons - more asymmetric photon distribution causing higher values of  $S_1$ ). It selects more backward emitted photons in the case when the reconstructed vertex is shifted in the direction along the electron momentum (counter balancing forward region populated by Cherenkov photons - more symmetric photon distribution causing smaller values of  $S_1$ ).

**Solution to this problem would be a better selection criteria of early light. It has to preserve high admixture of the Cherenkov photons, but needs to select scintillation photons in a more uniform manner. Working on it, but may not be simple so I don't want to include it in this paper.**

Good vertex resolution is essential for spherical harmonics analysis. Such strong

---

<sup>2</sup>We use average index of refraction of  $n=1.53$

226 dependence on the vertex resolution can be addressed by choosing a different liquid  
227 scintillator mixture with a more delayed emission of the scintillation light. Figure ??  
228 shows spherical harmonics calculated for the time profile which has scintillation com-  
229 ponent delayed by 0.5ns with respect to what is shown in Fig. 3

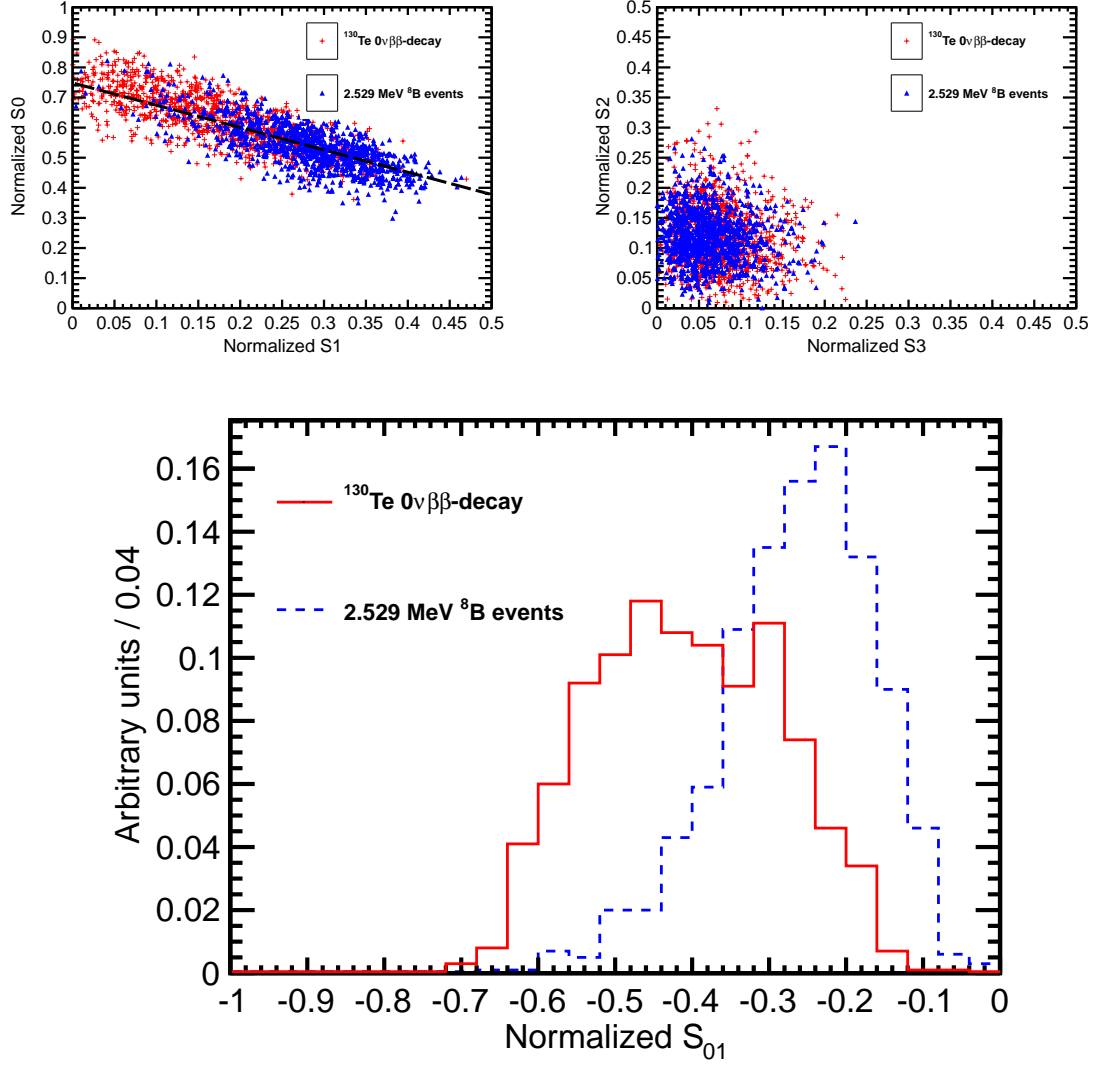


Figure 13: Spherical harmonics comparison between  $^{130}\text{Te } 0\nu\beta\beta\text{-decay}$  signal ( $Q=2.529$  MeV) (red) and  $^8\text{B}$  solar neutrinos background (blue) for 1000 simulated events originated at the center of the sphere.  $^8\text{B}$  events are implemented as 2.529 MeV electrons with initial direction along  $x$ -axis. Perfect vertex reconstruction - true vertex position is used. Time cut of 33.5 ns on the photon arrival time is applied. (Top left)  $S_0$  versus  $S_1$  scatter plot. Black dotted line is a linear fit of these 2D histograms. Variable  $S_{01}$  is defined as a projection of 2D distribution onto this linear fit. (Top right)  $S_2$  versus  $S_3$  scatter plot. (Bottom)  $S_{01}$  distribution for the signal and background.

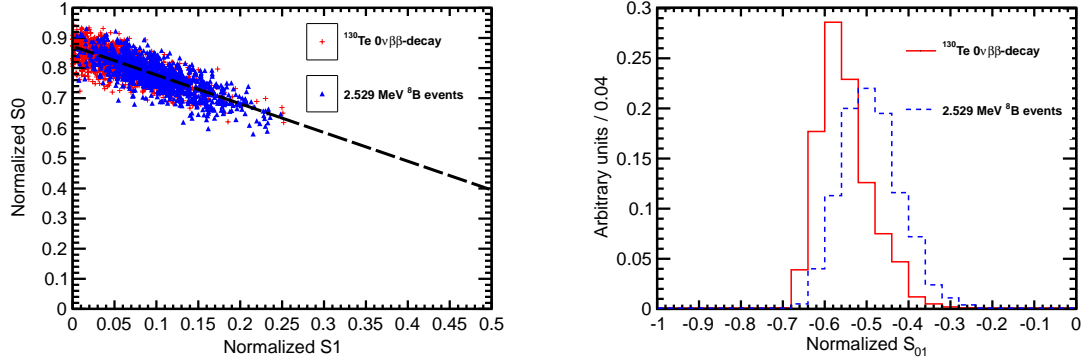


Figure 14: Spherical harmonics comparison between  $^{130}\text{Te}$   $0\nu\beta\beta$ -decay signal ( $Q=2.529$  MeV) (red) and  $^8\text{B}$  solar neutrinos background (blue) for 1000 simulated events. Vertices are uniformly distributed within the fiducial volume,  $R < 3$  m.  $^8\text{B}$  events are implemented as 2.529 MeV electrons with the initial momentum direction uniformly distributed within  $4\pi$  solid angle. Perfect vertex reconstruction - true vertex position is used. (Left)  $S_0$  versus  $S_1$  scatter plot. Black dotted line is a linear fit of these 2D histograms. Variable  $S_{01}$  is defined as a projection of 2D distribution onto this linear fit. (Right)  $S_{01}$

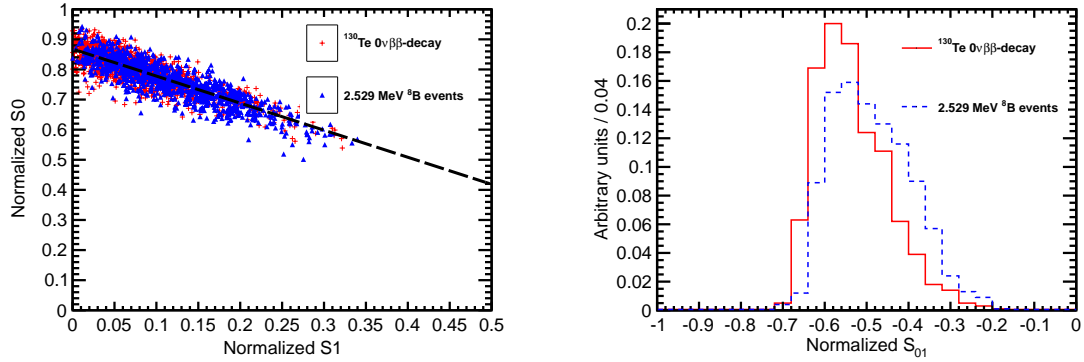


Figure 15: Spherical harmonics comparison between  $^{130}\text{Te}$   $0\nu\beta\beta$ -decay signal ( $Q=2.529$  MeV) (red) and  $^8\text{B}$  solar neutrinos background (blue) for 1000 simulated events. Vertices are uniformly distributed within the fiducial volume,  $R < 3$  m.  $^8\text{B}$  events are implemented as 2.529 MeV electrons with the initial momentum direction uniformly distributed within  $4\pi$  solid angle. Vertex is smeared with 3 cm resolution. (Left)  $S_0$  versus  $S_1$  scatter plot. Black dotted line is a linear fit of these 2D histograms. Variable  $S_{01}$  is defined as a projection of 2D distribution onto this linear fit. (Right)  $S_{01}$

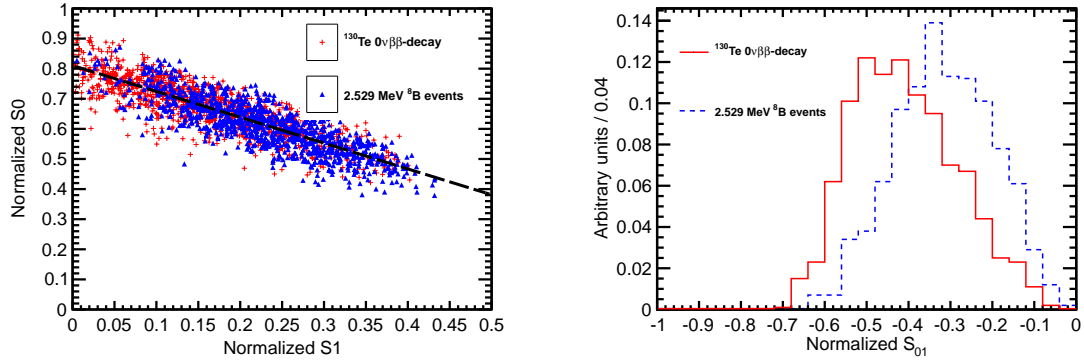


Figure 16: Spherical harmonics comparison between  $^{130}\text{Te}$   $0\nu\beta\beta$ -decay signal ( $Q=2.529$  MeV) (red) and  $^8\text{B}$  solar neutrinos background (blue) for 1000 simulated events. Vertices are uniformly distributed within the fiducial volume,  $R < 3$  m.  $^8\text{Be}$  events are implemented as 2.529 MeV electrons with the initial momentum direction uniformly distributed within  $4\pi$  solid angle. Vetrex is smeared with 3 cm resolution. **Scintillation light is delayed by additional 0.5 ns.** (Left)  $S_0$  versus  $S_1$  scatter plot. Black dotted line is a linear fit of these 2D histograms. Variable  $S_{01}$  is defined as a projection of 2D distribution onto this linear fit. (Right)  $S_{01}$

## 5 Conclusions

A technique based on spherical harmonics analysis is discussed to separate  $0\nu\beta\beta$ -decay from  ${}^8B$  solar neutrino interactions. The separation is based on distinct event topologies of signal and background. This event topology information is available in addition to the measurements of the energy deposited in the detector. This technique may be further developed and adopted by future large scale liquid scintillator detectors to suppress background coming from  ${}^8B$  solar neutrino interactions in the detector volume. The performance of the technique is mostly affected by chromatic dispersions, vertex reconstruction and time profile of the emission of the scintillation light. We show that a liquid scintillator detector with a  $\sim 1$  ns total delay of the scintillation light with respect to the Cherenkov light allows for use of spherical harmonics analysis as an extra handle to extract  $0\nu\beta\beta$ -decay signal.

## 6 Acknowledgments

To be finalized based on opt-in for the author list.

## A $0\nu\beta\beta$ -decay vs ${}^{10}C$ background

Other common backgrounds to  $0\nu\beta\beta$ -decay search include radioactive decays of nuclei excited by cosmic muons and decays of Th and U naturally present in the materials. In a liquid scintillator detectors most of events from Th and U decays are happening in the materials of the scintillator enclosure. Typically they enter the fiducial volume as 2.6 MeV gammas. These gammas either shower too late or have mis-reconstructed vertex. Both effects depend on details of a particular experiment and therefore in this paper we make no attempt to introduce a topology reconstruction for the backgrounds coming from Th and U lines. Cosmic induced backgrounds, to the contrary, are more generic and originate inside the fiducial volume. In this section we discuss

254 event topology of  $^{10}\text{C}$  events that are most relevant in the energy of 2-3 MeV.

255 Typical energy deposition by  $^{10}\text{C}$  events is shown in Fig. 17. We propose to use  
 256 spherical harmonics analysis to separate  $0\nu\beta\beta$ -decay events from  $^{10}\text{C}$  events that within  
 257 energy resolution overlap with the  $0\nu\beta\beta$ -decay Q-value.

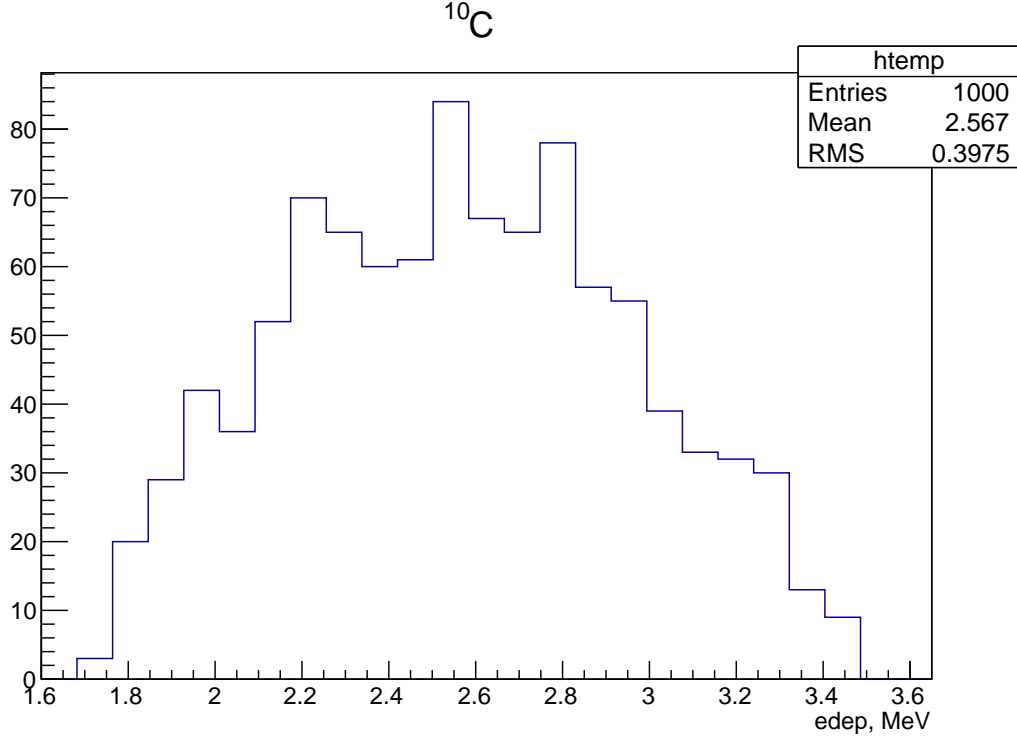


Figure 17: Energy deposition in  $^{10}\text{C}$  events.

258 We note that 98% of  $^{10}\text{C}$  decays through the excited state of  $^{10}\text{B}(718)$  that has  
 259 a half-life time of  $\sim 1$  ns. Therefore majority of  $^{10}\text{C}$  events have a prompt positron  
 260 accompanied by a delayed 0.718 MeV gamma. This delayed gamma affects PEs arrival  
 261 time distribution. Figure 18 shows shape comparison of PEs arrival time distribution  
 262 between  $^{130}\text{Te}$   $0\nu\beta\beta$ -decay and  $^{10}\text{C}$  events. Time profile of the scintillation photons  
 263 can be used to separate signal from  $^{10}\text{C}$  events.

264 Comparison of spherical harmonics is shown in Fig. 19.  $^{10}\text{C}$  events are generated at  
 265 the center of the detector. True vertex position is used to apply a 33.5 ns time cut to  
 266 select photons for the spherical harmonics analysis. The separation is seen in S0 vs S1

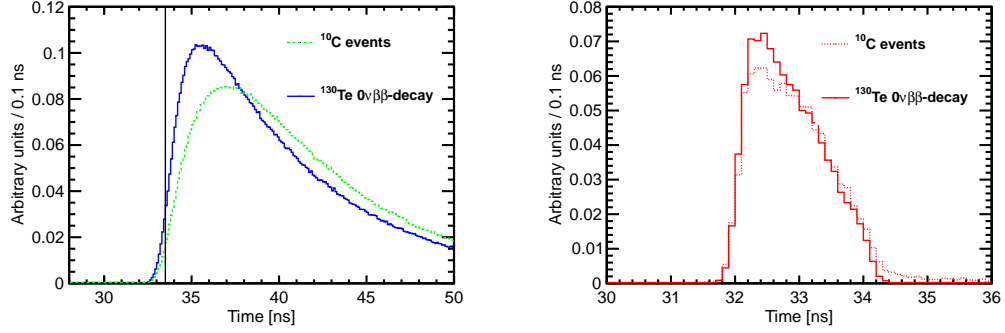


Figure 18: Photo-electron (PE) arrival times after application of the photo-detector transit time spread (TTS) of 100 ps for the simulation of 1000  $0\nu\beta\beta$ -decay events of  $^{130}\text{Te}$  (solid lines) and  $^{10}\text{C}$  (dotted lines) events at the center of the detector. All distributions are normalized for shape comparison. **Absolute number of PEs per event depends on the total energy deposited in the detector. Figure 17 shows energy deposited in the detector in  $^{10}\text{C}$  events.** (Left) Scintillation PEs arrival time. The black vertical line illustrates a time cut at 33.5 ns. (Right) Cherenkov PEs arrival time.

267 and S2 vs S3 scatter plots. We project both scatter plots to a line that gives maximum  
 268 separation (two bottom panels in Fig. 19).



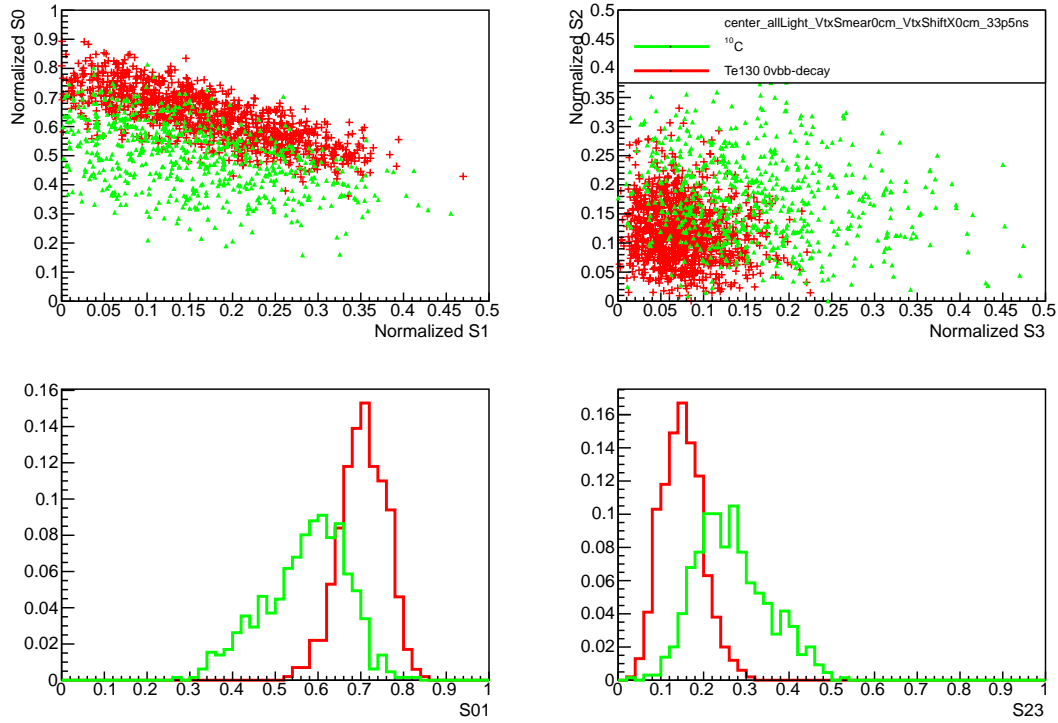


Figure 19: Spherical harmonics comparison between  $^{130}\text{Te}$   $0\nu\beta\beta$ -decay signal ( $Q=2.529$  MeV) (red) and  $^{10}\text{C}$  solar neutrinos background (blue) for 1000 simulated events originated at the center of the sphere.  $^{10}\text{C}$  with energy deposition between 2.1 MeV and 2.9 MeV are considered. Perfect vertex reconstruction - true vertex position is used. Time cut of 33.5 ns on the photon arrival time is applied. (Top left)  $S_0$  versus  $S_1$  scatter plot. (Top right)  $S_2$  versus  $S_3$  scatter plot. (Bottom left) Distribution of the  $S_{01}^{C10}$  variable calculated for signal (red) and background (green). (Bottom right) Distribution of the  $S_{23}^{C10}$  variable calculated for signal (red) and background (green).

## References

- [1] C. Aberle et al. JINST 9 P06012.
- [2] A good ref to SNO+ backgrounds description.